Efficient asymmetrical transmission through a metagrating for underwater acoustic waves

Hasna Kourchi, Simon Bernard, Farid Chati, Fernand Léon

Efficient asymmetrical transmission through a metagrating for underwater acoustic waves

Hasna Kourchi,[1] Simon Bernard,[1, a)] Farid Chati,[1] and Fernand Léon[1]
Laboratoire Ondes et Milieux Complexes (LOMC), UMR CNRS 6294, Université Le Havre Normandie, 75 rue Bellot, 76600, Le Havre, France

(Dated: 19 June 2023)

Acoustic asymmetrical transmission is a theoretical and engineering challenge because of the reciprocity of the linear acoustic wave equation. It can be achieved by systems breaking reciprocity, or by reciprocal systems relying solely on spatial symmetry breaking. Metagratings are planar structures relying on Bragg's diffraction to reroute wave energy towards a desired direction, and are eventually able to achieve asymmetrical transmission when build from an asymmetrical pattern of multiple basic elements. The challenge for water-like media is to combine the geometrical complexity of the structure with good acoustic impedance contrast and practical feasibility. In this work, we build a reciprocal metagrating from brass cylinders arranged according to a numerically optimized pattern, and obtain highly efficient asymmetrical transmission for underwater acoustic waves. Around 200 kHz, the structure transmits nearly all incident energy towards a 45° angle when insonified from one side, but act as a near perfect reflector when insonified from the other. The effect rely entirely on the simple phenomena of linear wave diffraction and interference. The generality and efficiency of this device could be of interest for applications in underwater acoustics or medical ultrasounds.

[a)]simon.bernard@univ-lehavre.fr

Asymmetrical transmission – a wave incident from one direction is transmitted, while a similar wave incident from the opposite direction is blocked – has many potential applications in acoustics, from one-way sound insulation to spurious echoes reduction in acoustic imaging. However, because of the reciprocity of the linear acoustic wave equation, such an effect is challenging to obtain[1]. For more than a decade, researchers have proposed various designs, either breaking reciprocity through non-linear effects[2–5], losses[6,7], spatiotemporal modulation[8], and rotating devices[9,10] or relying solely on spatial symmetry breaking using prisms[11–15], phononic crystals[16,17], and waveguides[18,19]. Planar acoustic metasurfaces can also achieve asymmetric transmission[20–24] with advantages regarding efficiency, complexity, and bulkiness. Phase-gradient metasurfaces are based on multiple small elements tailored to produce a spatially variable phase shift and reroute a wave towards a desired direction[25]. While efficient in air, the 3D-printed plastic labyrinth structures often employed to lengthen the wave path in metasurfaces are hardly adapted to water or water-like propagation media because of a poor acoustic impedance contrast. Furthermore, phase-gradient metasurfaces suffer from a limitation in their efficiency for large steering angles, due to the impossibility to match the impedance of the incident and outgoing waves[26,27].

Metagratings are structures composed of single repeated periodic cell instead of a gradient in properties, but can offer similar functionalities as phase-gradient metasurfaces with reduced fabrication complexity and unitary efficiency[28–30]. Metagratings rely entirely on Bragg's diffraction to open propagation modes in a finite set of directions. By engineering the element in the periodic cell, acoustic energy can be entirely directed towards a given mode. While originally proposed in electromagnetism[28], a growing number of studies report their use in acoustics[31–38]. Recently, multi-elements metagratings have been proposed as a way to leverage additional degrees-of-freedom in order to obtain a finer control over multiple diffraction modes[37,39]. A numerical study by Fan and Mei[37] demonstrates that the progressive addition of one element per periodic cell, up to four, opens up new ways of wavefront control with unitary efficiency, achieving perfect beam splitting, anomalous refraction and ultimately asymmetric transmission. Other studies add degrees-of-freedom by layering two metagratings to achieve the same effect[22,35].

Yet, despite promising design ideas and numerical studies, the challenge remains for water and water-like media to combine a precisely manufactured complex structure with a strong acoustic impedance contrast and practical feasibility. In this work, we build a reciprocal multi-element metagrating, based on the design idea of Fan and Mei[37], and show highly efficient asymmetrical transmission of underwater acoustic waves with a simple, passive, and planar device. The grating

is made from four brass cylinders per cell, whose geometrical arrangement is obtained through numerical optimization of a Finite Element model, with the objective to maximize transmission asymmetry. The structure is build from a pair of 3D-printed supports allowing one to position the high acoustic impedance cylinders according to the optimized pattern. The grating is then immersed in a water tank and studied under normal incidence for both directions. As a consequence of time-space reciprocity, the asymmetric effect is associated with a change in direction of the transmitted wave[1]. We finish the letter by illustrating how, by combining two gratings, it is possible for finite-width beams to correct for this direction change at the cost of a lateral shift in the beam axis.

Consider an infinite grating with period p, composed of four cylinders per periodic cell, and arranged as pictured in Fig. 1. A plane acoustic wave with frequency f is normally incident on the grating from the left or the right side. According to Bragg's law, waves are diffracted by such a periodic structure towards a finite number of modes whose directions θ_m satisfy :

$$\sin(\theta_m) = m\lambda/p \text{ with } m \text{ an integer.} \tag{1}$$

We here set the periodicity to $p = \sqrt{2}\lambda$, with wavelength $\lambda = c/f$, such that exactly six modes exist : $[R_{-1}, R_0, R_1, T_{-1}, T_0, T_1]$ with respective directions $[5\pi/4, \pi, 3\pi/4, -\pi/4, 0, \pi/4]$, the reference 0 angle being fixed as the direction of the normal transmit mode.

The amount of incident acoustic energy directed towards each mode depends on the scattering properties of the periodic cell. By careful design, it is possible to redirect all the incident energy towards a single mode among $[R_{-1}, R_0, R_1, T_{-1}, T_0, T_1]$. This is the working principle of metagratings[28]. In a simple case, such as reflection from a periodic grating made of a single small element, the amplitude of each mode can be analytically predicted, and the scattering element designed accordingly to obtain the desired effect[28,38]. In order to obtain complex effects such as the asymmetrical transmission targeted here, it is necessary to concurrently control a larger number of modes, which requires a large number of degrees-of-freedom in the design, and hence complex cell construction. In this case, analytically writing the mode become cumbersome, as multiple scattering occurs inside the cell, as well as between cells. However, as recently demonstrated[37], one can resort to numerical optimization to adjust the parameters of the grating in order to obtain the desired effect, and four cylinders per cell are sufficient to provide unidirectional transmission.

A frequency domain Finite Element (FE) model of the grating is build using Comsol Multiphysics Acoustic-Structure Interaction module. Four brass cylinders ($E = 100$ GPa, $\nu = 0.31$,

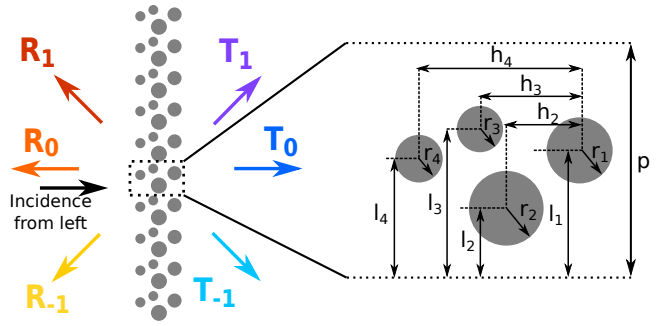

FIG. 1. Studied metagrating is composed of four brass cylinders per periodic cell. Given the grating periodicity p, 11 independent parameters are required to fully describe the arrangement, as pictured on the right. Periodicity is set so that three reflection $[R_{-1}, R_0, R_1]$ and three transmission modes $[T_{-1}, T_0, T_1]$ exist at $\pm 45^\circ$ from the normal. They are depicted here for normal incidence from the left side of the grating, but incidence from the right is also investigated, in which case the modes are flipped.

$\rho = 8500$ kg/m³) are immersed in a water background ($c = 1490$ m/s, $\rho = 1000$ kg/m³). Frequency is set to 200 kHz. Floquet periodic boundaries are used to model an infinite grating, and absorbing boundary conditions are used on the left and right boundaries. A normally incident plane wave with unitary amplitude is obtained as an ambient pressure field, incoming either from the left or right side. Transmit and reflection coefficients for each of the possible modes are obtained by integration over the left and right boundaries of the domain[27]. With four cylinders, there are 11 parameters to control (Fig. 1). Our objective here being to send all the energy to the first positive transmission order T_1, for a normally incident planar wave coming from the left and suppressing all the transmitted energy from an incidence wave from the right, a cost function is defined as

$$F = 1/T_1^{left} + (T_{-1}^{right} + T_0^{right} + T_1^{right}), \tag{2}$$

where $T_n^{left/right}$ denotes the energy transmittance towards the mode n for incidence from the left and right, respectively. Minimizing F should ensure a maximal transmitted energy towards the T_1 mode from incidence from the left, and minimum total transmission from incidence from the right side. The minimization process is run in two successive steps. First, a Nelder-Mead simplex optimization algorithm[40] (as implemented in the *fminsearch* function in Matlab) is used to minimize F by adjusting all of the 11 parameters of the cell. The algorithm is a heuristic search method that does not require derivative information, but is sensitive to the user-provided starting point for the search. The geometrical parameters obtained for a similar configuration of steel cylinders in a previous study[37] are therefore used as a starting point in the optimization

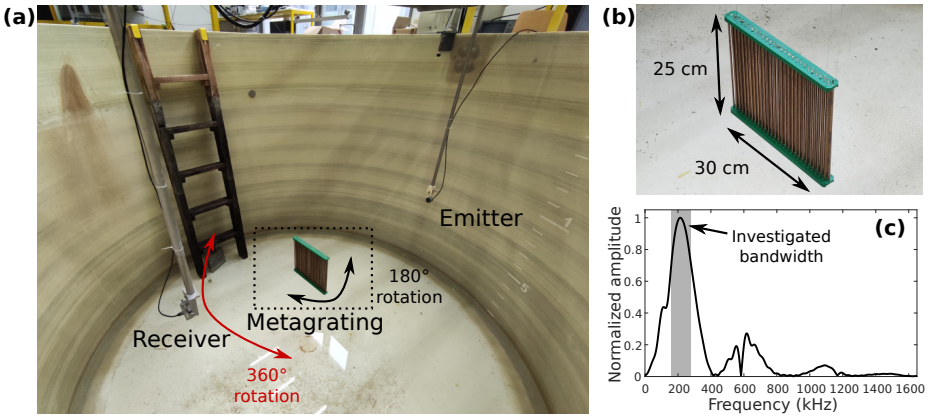

FIG. 2. (a) Experimental setup before filling-up the tank with water. The emitter is fixed, while the grating can be rotated by 180° to change incidence direction. The receiver can rotate around the grating in a full circle. (b) Close-up of the grating shows the brass tubes, hold in place by two 3D-printed supports designed according to the optimization process described in the main text. (c) Spectrum of the incident wave. Analysis is restricted to the high amplitude $160-280$ kHz band.

process, but with mechanical parameters of brass to reflect our experimental conditions. Brass being reasonably close from steel mechanically, this provides a good enough starting point for the algorithm to converge. In a second step, when a minimum of F is found, the optimized radii are fixed to the closest round value with 0.25 mm increments (as only those cylinders are available for the experiment), and the optimization run again with 7 free parameters. At the end of this process, we find the optimized parameters as follows: $r_1 = 0.175$ cm, $r_2 = 0.150$ cm, $r_3 = 0.125$ cm, $r_4 = 0.250$ cm, $h_2 = 1.115$ cm, $h_3 = 0.695$ cm, $h_4 = 0.555$ cm, $l_1 = 0.755$ cm, $l_2 = 0.750$cm, $l_3 = 0.905$ cm, $l_4 = 0.265$ cm, where (l_1, l_2, l_3, l_4) are the vertical coordinates of the cylinders and (h_2, h_3, h_4) are the horizontal distance between two cylinders (see Fig. 1). The total thickness is about 1.9 wavelength at 200 kHz. For this optimized configuration, the model predicts a 94.8% transmit efficiency (portion of transmitted energy) towards T_1 when incident from the left, and a 2.77% total transmit efficiency when incident from the right.

For the experimental implementation, two supports (green parts in Fig. 2) are build from Fused Filament Fabrication with poly-lactic acid (PLA) on a Prusa i3 MK3S+ 3D printer. The supports are designed as 300 mm long beams ($\approx$ 28 periods at 200 kHz in water), with 28x4 holes arranged according to the optimal configuration obtained above. Brass cylinders of appropriate radius, and 250 mm length, are then inserted in the support's holes to from the 250 by 300 mm grating. The 0.4 mm printer nozzle, governing the precision of the printer, is about 1/20th of a wavelength

at 200 kHz, which ensure that the actual fabricated grating is close to the optimal design. The experiment is carried out in a water tank (3 m diameter and 1.5 m depth), in which the target is suspended at mid-height as shown in Fig. 2-(a). Two identical ultrasound transducers (Panametrics v3507, 200 kHz central frequency, 51 mm diameter) are used. The first one, the acoustic source, is fixed at 1.4 m from the target. The second one, the receiver, is hold by a rotating arm at a distance of 0.4 m from the center of the tank. The grating itself can also be rotated to switch the incidence direction. With this configuration (transducer diameter, frequency, and distance) the insonified area is smaller than the metagrating, so that scattering on its edges is not a concern. A pulse generator (Panametrics 5052PR) is used to send a broadband signal and the response is recorded by an oscilloscope (HDO6034, Teledyne Lecroy) for each position of the receiver around the circumference with 2° steps. Signals are time windowed to isolate the reflected signal form the incident signal and to remove spurious reflections from the tank boundary (which is easy thanks to the large size of the tank) and the spectrum for each receiving position is normalized by a reference spectrum obtained from reflection on a stainless steel plate acting as a perfect reflector[38].

The results are presented in Fig. 3 for the $160-280$ kHz investigated bandwidth, and more specifically for the 200 kHz design frequency in Fig. 4. In Fig. 3, top panels (a-b) display the

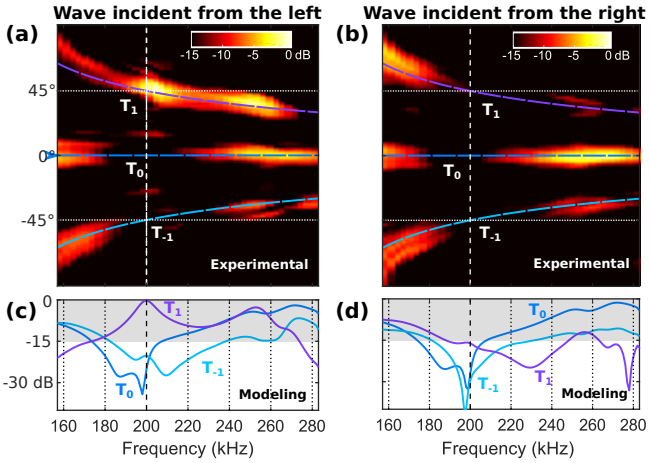

FIG. 3. Experimental (a, b) and FE modeling (c, d) results for the proposed metagrating under normally incident waves, from either the left (left panels) or right (right panels) side of the grating. For incidence from the left, the wave is almost totally transmitted by the grating around 200 kHz, towards the T_1 mode at 45°. In contrast, incidence from the right side results in almost zero transmission (< -15 dB). The colored dashed lines in (a-b) correspond to the angle predicted from Eq. 1 The prediction of the model (c, d) are in good agreement with the experimental results (a, b).

recorded acoustic pressure as a function of frequency and transmit angle for incidence from the left (a) and from the right (b), while the bottom panels (c-d) display the predicted transmittance from the FEM model. The angles predicted by eq. 1 are superimposed as dashed lines. The three possible propagation modes corresponding to the T_{-1}, T_0 and T_1 modes are clearly visible from the experimental data. The mode trajectories shows significant dips around 200 kHz, falling below the 15 dB dynamic range of the picture, for all modes except the T_1 mode for left incidence which display a strong maxima around 45°, in good quantitative agreement with the prediction from the FE model display below (c-d). In Fig. 4, the experimental results at 200 kHz are presented as polar plots for both incidence (a-b), and the results from the FE model as full wavefield pictures (c-d). The asymmetric response of the grating is particularly visible on the polar plots, with a single main lobe of strong amplitude directed towards the T_1 mode at 45° for incidence from the left (a), and two main lobes in reflection (R_0 and R_1) for incidence from the right (b). The full wavefields (c-d) pictures show a near perfect anomalous transmission towards an oblique direction for incidence from the left (c), and almost null transmission for incidence from the right (d). The decomposition in incident and scattered wavefields also reveals the physical process at play here : energy is actually scattered by the grating towards multiple directions, but the interference with the incident field cancel the wave in all but the desired direction.

The sums of the three transmittance $\sum T = T_{-1} + T_0 + T_1$, are plotted in Fig. 5-(a) for incidence from the left (blue) and from the right (red), both for experimental results (dashed lines) and numerical prediction (plain lines). The contrast ratio CR, calculated as[41]

$$CR = \frac{\sum T^{left} - \sum T^{right}}{\sum T^{left} + \sum T^{right}} \tag{3}$$

is also plotted on Fig. 5-(b). CR reaches 0.87 in experiment and 0.94 in the model at about 200 kHz, and is > 0.5 over a 22 kHz bandwidth (11% relative bandwidth). The agreement between the finite element model prediction and the experimental result over all the working frequency range of the transducer is remarkable, although the experimental contrast is slightly lower than the predicted contrast. This can be explained by beam spreading occurring experimentally, while the model assumes a perfect plane wave.

Note that with the setup used here, the receiver is at some point located in front of the emitter and potentially disturb the incoming wavefront due to scattering. This does likely affects the recorded pressure in reflection around the 180° mark displayed in Fig. 4 (a-b) but does not affect the results for transmitted waves (Fig. 3) nor the contrast ratio (Fig. 5).

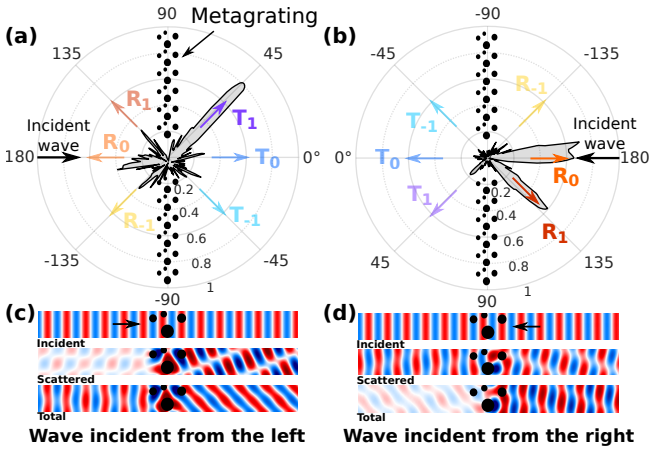

FIG. 4. (a-b) Experimental pressure at the metagrating design frequency of 200 kHz, normalized to the incident pressure, as a function of the receiving angle. The metagrating displays a strongly asymmetric behavior, with near total transmission toward a 45° angle for incidence from the left (a) and near total reflection towards the R_0 and R_1 modes (normal and anomalous reflection, respectively) for incidence from the right (b). The corresponding modeled pressure wavefield at 200 kHz (c-d) illustrate how the field scattered by the grating interfere with the incident wavefield to suppress some of the transmission and reflection modes to produce the desired effect.

The transmitted wave is associated with a change in direction. This is is a necessity for any asymmetric transmission system which does not rely on breaking the reciprocity of the wave equation. Indeed, lets suppose that no direction change occurs from a reciprocal asymmetric transmission system. Then, by flipping the device, or equivalently switching the source and receiver, one should obtain the exact same results due to reciprocity, and therefore no asymmetry. Said otherwise, the direction change is a fundamental consequence of reciprocity. However, it is possible for finite-width beams to correct for this direction change at the cost of a lateral shift in the beam axis, by combining two similar reciprocal metagratings and leveraging reversibility. This is illustrated on Fig. 6, which shows the results of a FE model in a infinite domain (radiation boundary conditions), with a finite width incident Gaussian beam. Two grating are used here, the one on the left being exactly the same as described above, except that it is there only 10 periods large, while the second is a 180° flipped version of the first. By reversibility of the reciprocal grating, the 45° incident wave on the second grating in Fig. 6-(a) is fully transmitted towards a 0° transmit angle. The wave incident from the right along the central beam axis is fully reflected by the left grating, achieving asymmetric transmission without a change in direction, at the cost of a shift in the beam

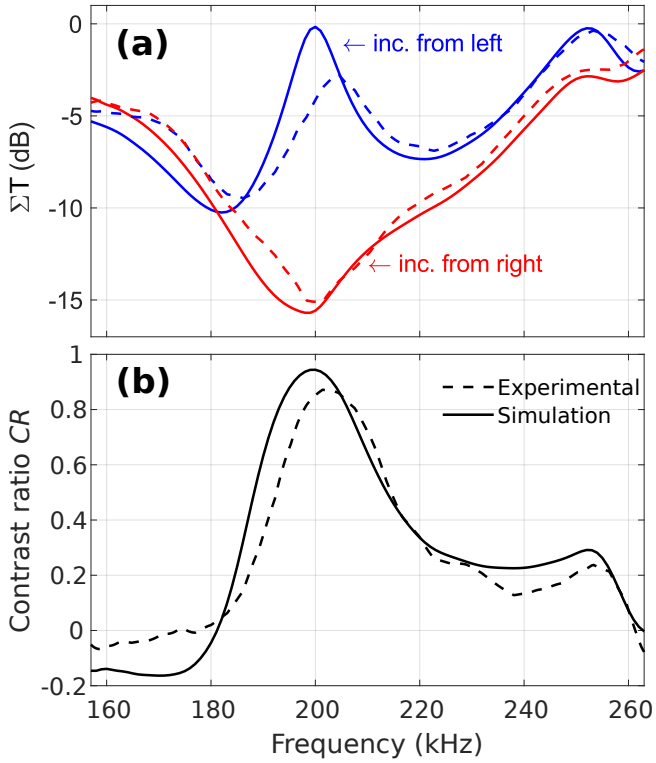

FIG. 5. (a) Sum of the transmission efficiency T over the three modes $\{-1,0,1\}$ for incidence from the left (blue) and from the right (red) and (b) contrast ratio of left/right transmission. The experimental results (dashed lines) match well to the FEM prediction (solid lines) over the studied bandwidth. The contrast reach 0.87 experimentally and 0.94 in the model at 200 kHz, and is > 0.5 over a 22 kHz bandwidth (11% relative bandwidth).

axis and a less compact system.

In this work, we designed, built and tested a planar, passive, and thin acoustic metagrating that achieve asymmetrical transmission with good contrast for acoustic waves underwater. Around 200 kHz, it achieves almost perfect transmission towards a slanted angle for wave incident from one side, and near total reflection for waves incident from the other side. We foresee that it could find applications in underwater acoustics for communication, noise mitigation, or stealth. As ultrasound waves in soft tissues mostly behaves like in water, it might also be useful in medical ultrasonic to reduce spurious echoes in imaging or to protect the source from back-scattered waves in high intensity therapeutic ultrasound. Finally, we emphasis that the proposed grating rely entirely on linear acoustic wave scattering and interference, two universal phenomena occurring at all frequencies in all propagation media. The proposed grating could therefore be scaled to any

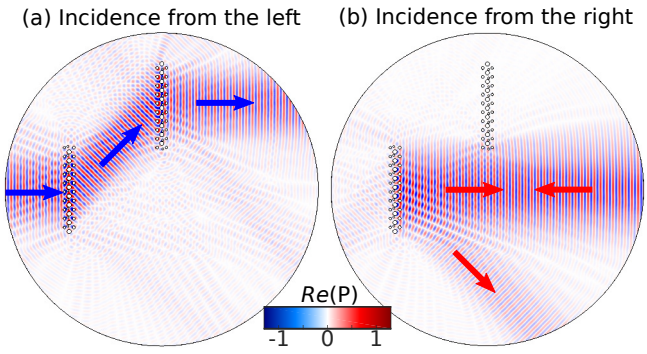

FIG. 6. FEM results for combining two metagratings. The acoustic total pressure field (real part) is represented for a unit amplitude incident Gaussian beam, either from the left (a) or from the right (b). The leftmost grating (in both pictures) is the same as studied above in the paper, except that it is only 10 periods large, and the second grating is a 180° rotated version of the first. Leveraging reversibility, it is possible to trade the direction change of the transmitted wave for a lateral shift in the beam axis.

frequency range, and adapted to work in other media such as air, where high acoustic impedance contrast is easy to obtain. The effect could also be potentially obtained for other kind of mechanical waves such as elastic waves in solids or surface water waves. This will be a subject of future research.

ACKNOWLEDGMENTS

This work received financial support from the Region Normandie (Project No. R2019-RIN-0027). We thank H. Cahingt, F. Duhamel and N. Jafar for their help in setting up the experiment.

DATA AVAILABILITY

The data that support the findings of this study are available from the corresponding author upon reasonable request.

REFERENCES

[1]A. Maznev, A. Every, and O. Wright, "Reciprocity in reflection and transmission: What is a 'phonon diode'?" Wave Motion **50**, 776–784 (2013).

[2]B. Liang, B. Yuan, and J. C. Cheng, "Acoustic diode: Rectification of acoustic energy flux in one-dimensional systems," Physical review letters **103**, 104301 (2009).

[3]B. Liang, X. S. Guo, J. Tu, D. Zhang, and J. C. Cheng, "An acoustic rectifier," Nature materials **9**, 989–992 (2010).

[4]T. Devaux, V. Tournat, O. Richoux, and V. Pagneux, "Asymmetric acoustic propagation of wave packets via the self-demodulation effect," Physical review letters **115**, 234301 (2015).

[5]T. Devaux, A. Cebrecos, O. Richoux, V. Pagneux, and V. Tournat, "Acoustic radiation pressure for nonreciprocal transmission and switch effects," Nature Communications **10**, 3292 (2019).

[6]Y. Li, C. Shen, Y. Xie, J. Li, W. Wang, S. A. Cummer, and Y. Jing, "Tunable asymmetric transmission via lossy acoustic metasurfaces," Physical review letters **119**, 035501 (2017).

[7]F. Ju, Y. Tian, Y. Cheng, and X. Liu, "Asymmetric acoustic transmission with a lossy gradient-index metasurface," Applied Physics Letters **113**, 121901 (2018).

[8]Z. Chen, Y. Peng, H. Li, J. Liu, Y. Ding, B. Liang, X. F. Zhu, Y. Lu, J. C. Cheng, and A. Alù, "Efficient nonreciprocal mode transitions in spatiotemporally modulated acoustic metamaterials," Science advances **7**, eabj1198 (2021).

[9]R. Fleury, D. L. Sounas, C. F. Sieck, M. R. Haberman, and A. Alù, "Sound isolation and giant linear nonreciprocity in a compact acoustic circulator," Science **343**, 516–519 (2014).

[10]Q. Wang, Z. Zhou, D. Liu, H. Ding, M. Gu, and Y. Li, "Acoustic topological beam nonreciprocity via the rotational doppler effect," Science Advances **8**, eabq4451 (2022).

[11]J. Hwan Oh, H. Woong Kim, P. Sik Ma, H. Min Seung, and Y. Young Kim, "Inverted bi-prism phononic crystals for one-sided elastic wave transmission applications," Applied Physics Letters **100**, 213503 (2012).

[12]Y. Li, B. Liang, Z. M. Gu, X. Y. Zou, and J. C. Cheng, "Unidirectional acoustic transmission through a prism with near-zero refractive index," Applied Physics Letters **103**, 053505 (2013).

[13]Z. M. Gu, B. Liang, X. Y. Zou, J. Yang, Y. Li, J. Yang, and J. C. Cheng, "One-way acoustic mirror based on anisotropic zero-index media," Applied Physics Letters **107**, 213503 (2015).

[14]A. Song, J. Li, C. Shen, X. Peng, X. Zhu, T. Chen, and S. A. Cummer, "Broadband high-index prism for asymmetric acoustic transmission," Applied Physics Letters **114**, 121902 (2019).

[15]Y. Wang, J. P. Xia, H.-x. Sun, S. Q. Yuan, Y. Ge, Q. R. Si, Y. J. Guan, and X. J. Liu, "Multifunctional asymmetric sound manipulations by a passive phased array prism," Physical Review Applied **12**, 024033 (2019).

[16]X. Zhu, X. Zou, B. Liang, and J. C. Cheng, "One-way mode transmission in one-dimensional phononic crystal plates," Journal of Applied Physics **108**, 124909 (2010).

[17]A. Cicek, O. Adem Kaya, and B. Ulug, "Refraction-type sonic crystal junction diode," Applied Physics Letters **100**, 111905 (2012).

[18]B. Yuan, B. Liang, J. C. Tao, X. Y. Zou, and J. C. Cheng, "Broadband directional acoustic waveguide with high efficiency," Applied Physics Letters **101**, 043503 (2012).

[19]Y. F. Zhu, X. Y. Zou, B. Liang, and J. C. Cheng, "Broadband unidirectional transmission of sound in unblocked channel," Applied Physics Letters **106**, 173508 (2015).

[20]Y. F. Zhu, X. Y. Zou, B. Liang, and J. C. Cheng, "Acoustic one-way open tunnel by using metasurface," Applied Physics Letters **107**, 113501 (2015).

[21]C. Shen, Y. Xie, J. Li, S. A. Cummer, and Y. Jing, "Asymmetric acoustic transmission through near-zero-index and gradient-index metasurfaces," Applied Physics Letters **108**, 223502 (2016).

[22]B. Liu and Y. Jiang, "Controllable asymmetric transmission via gap-tunable acoustic metasurface," Applied Physics Letters **112**, 173503 (2018).

[23]Y. Qian, J. Yang, and J. Hu, "Angle-dependent broadband asymmetric acoustic transmission in a planar device," Scientific Reports **12**, 18421 (2022).

[24]B. Xie, H. Cheng, K. Tang, Z. Liu, S. Chen, and J. Tian, "Multiband asymmetric transmission of airborne sound by coded metasurfaces," Physical Review Applied **7**, 024010 (2017).

[25]B. Assouar, B. Liang, Y. Wu, Y. Li, J. C. Cheng, and Y. Jing, "Acoustic metasurfaces," Nature Reviews Materials **3**, 460–472 (2018).

[26]N. M. Estakhri and A. Alu, "Wave-front transformation with gradient metasurfaces," Physical Review X **6**, 041008 (2016).

[27]A. Díaz-Rubio and S. A. Tretyakov, "Acoustic metasurfaces for scattering-free anomalous reflection and refraction," Physical Review B **96**, 125409 (2017).

[28]Y. Ra'di, D. L. Sounas, and A. Alù, "Metagratings: Beyond the limits of graded metasurfaces for wave front control," Physical review letters **119**, 067404 (2017).

[29]A. Epstein and O. Rabinovich, "Unveiling the properties of metagratings via a detailed analytical model for synthesis and analysis," Physical Review Applied **8**, 054037 (2017).

[30]D. Torrent, "Acoustic anomalous reflectors based on diffraction grating engineering," Physical Review B **98**, 060101 (2018).

[31]Z. Hou, X. Fang, Y. Li, and B. Assouar, "Highly efficient acoustic metagrating with strongly coupled surface grooves," Physical Review Applied **12**, 034021 (2019).

[32]Y. Fu, C. Shen, Y. Cao, L. Gao, H. Chen, C. T. Chan, S. A. Cummer, and Y. Xu, "Reversal of transmission and reflection based on acoustic metagratings with integer parity design," Nature communications **10**, 2326 (2019).

[33]Y. Fu, Y. Cao, and Y. Xu, "Multifunctional reflection in acoustic metagratings with simplified design," Applied Physics Letters **114**, 053502 (2019).

[34]Y. K. Chiang, S. Oberst, A. Melnikov, L. Quan, S. Marburg, A. Alù, and D. A. Powell, "Reconfigurable acoustic metagrating for high-efficiency anomalous reflection," Physical Review Applied **13**, 064067 (2020).

[35]Y. Y. Fu, J. Q. Tao, A. L. Song, Y.-W. Liu, and Y. D. Xu, "Controllably asymmetric beam splitting via gap-induced diffraction channel transition in dual-layer binary metagratings," Frontiers of Physics **15**, 1–6 (2020).

[36]A. Melnikov, M. Maeder, N. Friedrich, Y. Pozhanka, A. Wollmann, M. Scheffler, S. Oberst, D. Powell, and S. Marburg, "Acoustic metamaterial capsule for reduction of stage machinery noise," The Journal of the Acoustical Society of America **147**, 1491–1503 (2020).

[37]L. Fan and J. Mei, "Metagratings for waterborne sound: Various functionalities enabled by an efficient inverse-design approach," Physical Review Applied **14**, 044003 (2020).

[38]S. Bernard, F. Chikh-Bled, H. Kourchi, F. Chati, and F. Léon, "Broadband negative reflection of underwater acoustic waves from a simple metagrating: modeling and experiment," Physical Review Applied **17**, 024059 (2022).

[39]Y. Ra'di and A. Alù, "Metagratings for efficient wavefront manipulation," IEEE Photonics Journal **14**, 1–13 (2021).

[40]J. C. Lagarias, J. A. Reeds, M. H. Wright, and P. E. Wright, "Convergence properties of the nelder–mead simplex method in low dimensions," SIAM Journal on optimization **9**, 112–147 (1998).

[41]X.-F. Li, X. Ni, L. Feng, M.-H. Lu, C. He, and Y.-F. Chen, "Tunable unidirectional sound propagation through a sonic-crystal-based acoustic diode," Physical review letters **106**, 084301 (2011).